A Stochastic Projection Method for Microchannel Flow

O.P. Le Maître*, O.M. Knio**, R.G. Ghanem*** and H.N. Najm****

* CEMIF, Université d'Evry Val d'Essone
91020 Evry, France, olm@aramis.iup.univ-evry.fr
** Department of Mechanical Engineering, Johns Hopkins University
Baltimore, MD 21218, USA, knio@jhu.edu
*** Department of Civil Engineering, Johns Hopkins University
Baltimore, MD 21218, USA, ghanem@jhu.edu
**** Combustion Research Facility, Sandia National Laboratories,
Livermore, CA 94550, USA, hnnajm@ca.sandia.gov

ABSTRACT

The construction and implementation of a stochastic flow solver is described. The solver combines a spectral stochastic uncertainty representation scheme with a finite difference projection method for flow simulation. The uncertainty quantification scheme is based on representing the stochastic dependence of the solution in terms of the Polynomial Chaos system, and the coefficients in this representation are obtained using a Galerkin approach. It is shown that incorporation of the spectral uncertainty representation scheme into the projection method results in a coupled system of advection-diffusion equations for the various uncertainty fields, and in a *decoupled* system of pressure projection steps. This leads to a very efficient stochastic solver, whose advantages are illustrated using transient simulations of transport and mixing in a microchannel.

Keywords: Stochastic, Polynomial Chaos, Projection, Navier-Stokes, Uncertainty.

1 INTRODUCTION

The simulation of microfluid systems is often complicated due to uncertainties in material properties as well as initial and boundary conditions. Thus, in order to become effective tools, it is essential for simulation-based design approaches to include a rational assessment of these uncertainties. Typically, uncertainty quantification is based on Monte-Carlo (MC) approaches [1], [2] which rely on repeated model computations to span the relevant parameter ranges. However, this approach can be impractical for complex models with many uncertain parameters, and it does not generally provide adequate information on sensitivities. On the other hand, the stochastic spectral finite element method (SSFEM) provides a potentially more efficient approach to uncertainty quantification. The key concept in SSFEM [3] is to consider the uncertainty as generating a new dimension, and to regard the solution as being dependent on this dimension. A convergent expansion along the new dimension is then sought in terms of the Polynomial Chaos system [4], [5], and the coefficients in this representation are determined through a weighted residual formalism. So far, SSFEM has been primarily applied in structural and soil applications, but has not yet been applied to fluid problems involving advection, mixing or chemical reactions.

This paper focuses on the adaptation of the SSFEM methodology to microchannel flow. We briefly outline the construction of a numerical scheme that incorporates the spectral stochastic uncertainty representation with a finite-difference projection method for flow simulation [6]. This results in a stochastic projection method (SPM) whose implementation is illustrated in light of simulations of transport and mixing in microchannel flow. For brevity, we restrict our attention to a general Navier-Stokes construction. This formulation, however, can be readily adapted to an unsteady (or pseudo-transient) Stokes flow formulation.

2 APPROACH

2.1 Governing Equations

We consider 2D flow, in the (x, y) plane, of a uniform-density, thermally-stratified, Newtonian fluid inside a narrow channel of height H and width B. The evolution of the flow within the channel is governed by the mass, momentum, and energy conservation equations:

$$\boldsymbol{\nabla} \cdot \boldsymbol{u} = 0 \tag{1}$$

$$\frac{\partial \boldsymbol{u}}{\partial t} + (\boldsymbol{u} \cdot \boldsymbol{\nabla})\boldsymbol{u} = -\boldsymbol{\nabla} p + \boldsymbol{\nabla} \cdot \left[\nu \overline{\boldsymbol{S}}\right] \tag{2}$$

$$\frac{\partial T}{\partial t} + \boldsymbol{\nabla} \cdot (\boldsymbol{u} T) = \boldsymbol{\nabla} \cdot (\lambda \boldsymbol{\nabla} T) \tag{3}$$

where $\boldsymbol{u}$ is the velocity field, $\tilde{p}$ is the pressure, ρ is the density, $p \equiv \tilde{p}/\rho$, ν is the kinematic viscosity, $\overline{\boldsymbol{S}}$ is the strain rate tensor, T is temperature and λ is the thermal diffusivity.

To illustrate the proposed approach, we focus on the case of uncertain transport properties and boundary conditions, and restrict our attention to stochastic processes generated by Gaussian random variables. Within this context, we consider the simulation of transport and mixing in the double-inlet microchannel schematically illustrated in figure 1. The second inlet stream has uncertain temperature, modelled as a Gaussian random variable with standard deviation of $0.1T_{ref}$, where T_{ref} is the mean temperature. Meanwhile, the dependence of the viscosity on temperature is given by:

$$\frac{\nu(\boldsymbol{x})}{\nu_0} = 1 + K'(T(\boldsymbol{x}) - T_{ref}) \tag{4}$$

where $\nu_0 \equiv \nu(T_{ref})$, and K' is a constant that reflects the sensitivity of the viscosity on temperature variation.

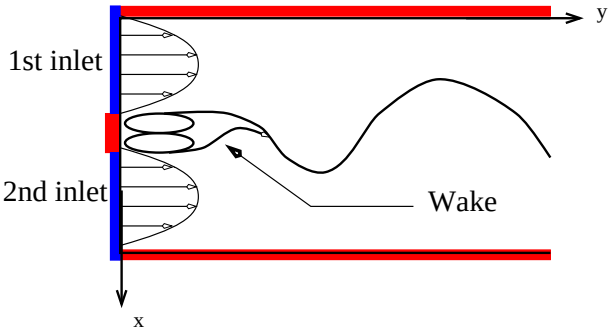

Figure 1: Schematic illustration of the double-inlet microchannel.

2.2 Stochastic Formulation

We rely on the polynomial chaos expansion of the stochastic fields:

$$T(\boldsymbol{x},t,\theta) = \sum_{i=0}^{P} T_i(\boldsymbol{x},t)\Psi_i(\theta) \tag{5}$$

$$\boldsymbol{u}(\boldsymbol{x},t,\theta) = \sum_{i=0}^{P} \boldsymbol{u}_i(\boldsymbol{x},t)\Psi_i(\theta) \tag{6}$$

$$p(\boldsymbol{x},t,\theta) = \sum_{i=0}^{P} p_i(\boldsymbol{x},t)\Psi_i(\theta) \tag{7}$$

$$\nu(\boldsymbol{x},t,\theta) = \nu_0(1-K) + \nu_0 K' \sum_{i=0}^{P} T_i(\boldsymbol{x},t)\Psi_i(\theta) \tag{8}$$

where $K \equiv K'T_{ref}$, P is the order of the polynomial chaos expansion, and the argument θ is used to denote the probabilistic character of the corresponding field.

Introducing (5) into the energy equation, multiplying by Ψ_k and evaluating the expectation, we get:

$$\frac{\partial T_k}{\partial t} + \sum_{i=0}^{P}\sum_{j=0}^{P} C_{ijk}\boldsymbol{u}_i \cdot \boldsymbol{\nabla} T_j = \lambda \nabla^2 T_k \tag{9}$$

where the expectation is defined according to:

$$\langle f \rangle = \frac{1}{\sqrt{2\pi}} \int_{-\infty}^{\infty} f(\xi) \exp\left(-\frac{\xi^2}{2}\right) d\xi \tag{10}$$

and

$$C_{ijk} \equiv \frac{< \Psi_i \Psi_j \Psi_k >}{< \Psi_k \Psi_k >} \tag{11}$$

are constants that are independent of the solution. In a similar fashion, we introduce (6–8) into the Navier-Stokes equations and perform a similar decomposition to obtain:

$$\frac{\partial \boldsymbol{u}_k}{\partial t} + \sum_{i=0}^{P}\sum_{j=0}^{P} C_{ijk}(\boldsymbol{u}_i \cdot \boldsymbol{\nabla})\boldsymbol{u}_j = \nu_0(1-K)\nabla^2 \boldsymbol{u}_k + \nu_0 K' \sum_{i=0}^{P}\sum_{j=0}^{P} C_{ijk} \boldsymbol{\nabla} \cdot \left(T_j \overline{\boldsymbol{S}}(\boldsymbol{u}_i)\right) - \boldsymbol{\nabla} p_k \tag{12}$$

together with the divergence constraints:

$$\boldsymbol{\nabla} \cdot \boldsymbol{u}_k = 0 \tag{13}$$

Note that a transient Stokes flow formulation can be obtained simply by ignorning the convective acceleration terms in Eq. (12).

2.3 Solution Scheme

Our approach to the formulation of the stochastic solver is based on the observation that the velocity divergence constraints are *decoupled*, and this suggests the implementation of a projection-type scheme [7] in which the advection and diffusion terms are integrated in a first fractional step, and the divergence constraints are then enforced in a second fractional step. Since the pressure terms and divergence constraints are decoupled, this approach results in a set of $P+1$ decoupled pressure projection steps. Since these steps typically account for the bulk of the computational effort in incompressible flow simulations, the solution of the stochastic system can be obtained at essentially a cost of $P+1$ deterministic solutions.

The present formulation of the stochastic solution scheme adapts elements of previously developed low-Mach-number solvers in [8], [9]. We rely on discretization of all fields variables using a uniform Cartesian mesh with cell size Δx and Δy in the x and y directions, respectively. The velocity modes $\boldsymbol{u}_k$ are defined on cell edges, while the scalar fields p_k, T_k, and ν_k are

defined on cell centers. Spatial derivatives are approximated using second-order centered differences.

The governing equations are integrated using a fractional step projection scheme. In the first fractional step, we integrate the coupled advection-diffusion equations:

$$\frac{\partial \boldsymbol{u}_k}{\partial t} + \sum_{i=0}^{P}\sum_{j=0}^{P} C_{ijk}(\boldsymbol{u}_i \cdot \boldsymbol{\nabla})\boldsymbol{u}_j = \nu_0(1-K)\nabla^2 \boldsymbol{u}_k + \nu_0 K' \sum_{i=0}^{P}\sum_{j=0}^{P} C_{ijk}\,\boldsymbol{\nabla}\cdot\left(T_j \overline{\boldsymbol{S}}(\boldsymbol{u}_i)\right) \quad (14)$$

for $k = 0, \ldots, P$. The explicit, second-order Adams-Bashforth scheme is used for this purpose; we thus have:

$$\frac{\boldsymbol{u}_k^* - \boldsymbol{u}_k^n}{\Delta t} = \frac{3}{2}\boldsymbol{H}_k^n - \frac{1}{2}\boldsymbol{H}_k^{n-1} \qquad k = 0, \ldots, P \quad (15)$$

where $\boldsymbol{u}_k^*$ are the predicted velocity modes, Δt is the time step,

$$\boldsymbol{H}_k \equiv \nu_0(1 - K'T_{ref})\nabla^2 \boldsymbol{u}_k + \sum_{i=0}^{P}\sum_{j=0}^{P} C_{ijk}\left[\nu_0 K' \boldsymbol{\nabla}\cdot\left(T_j\overline{\boldsymbol{S}}(\boldsymbol{u}_i)\right) - (\boldsymbol{u}_i\cdot\boldsymbol{\nabla})\boldsymbol{u}_j\right], \quad (16)$$

and the superscripts refer to the time level. A similar treatment is used for the energy equation, which is integrated using:

$$\frac{T_k^{n+1} - T_k^n}{\Delta t} = \frac{3}{2}J_k^n - \frac{1}{2}J_k^{n-1} \qquad k = 0, \ldots, P \quad (17)$$

where

$$J_k \equiv \lambda\nabla^2 T_k - \sum_{i=0}^{P}\sum_{j=0}^{P} C_{ijk}\boldsymbol{u}_i \cdot \boldsymbol{\nabla} T_j \quad (18)$$

In the second fractional step, we perform a pressure correction to the predicted velocity in order to satisfy the divergence constraints. Specifically, we have:

$$\frac{\boldsymbol{u}_k^{n+1} - \boldsymbol{u}_k^*}{\Delta t} = -\boldsymbol{\nabla} p_k \qquad k = 0, \ldots, P \quad (19)$$

where the pressure fields p_k are determined so that the fields $\boldsymbol{u}_k^{n+1}$ satisfy the divergence constraints in (13), i.e.

$$\boldsymbol{\nabla}\cdot\boldsymbol{u}_k^{n+1} = 0 \quad (20)$$

Combining equations (19) and (20) results in the following system of *decoupled* Poisson equations:

$$\nabla^2 p_k = -\frac{1}{\Delta t}\boldsymbol{\nabla}\cdot\boldsymbol{u}_k^* \qquad k = 0, \ldots, P \quad (21)$$

Similar to the original projection method, the above Poisson equations are solved, independently, subject to Neumann conditions that are obtained by projecting equation (19) in the direction normal to the domain boundary [7], [10]. A fast, Fourier-based solver is employed for the inversion of the discrete Poisson operator.

3 RESULTS

In the simulations, the channel inlet consists of two streams having identical parabolic velocity profiles with peak velocity V_{ref}. The two inlet streams are separated by a plate of thickness D. The flow is characterized by the Reynolds number $Re \equiv V_{ref}B/\nu_0$, the blockage ratio D/B, and the Prandtl number λ/ν_0. Here, $\nu_0 \equiv \nu(T_{ref})$ is the reference viscosity. Note that the blockage ratio and Re can be combined to define a Reynolds number based on the plate thickness, $Re_D \equiv V_{ref}D/\nu_0 = ReD/B$. If Re_D is large enough the wake of the plate is unstable and periodic vortex shedding is observed, at least for small downstream distances. This situation arises in the example below, where $D/B = 0.2$, $Re = 826$, and $Re_D = 165.2$. Results are obtained for different values of K, $K = 0.1$, 0.2 and 0.4. In all cases, the Prandtl number $\lambda/\nu_0 = 6$. The computations are performed in a domain with height $H = 5B$, using a 100×352 grid, a time step $\Delta t V_{ref}/B = 2 \times 10^{-3}$ and a polynomial chaos expansion with $P = 3$.

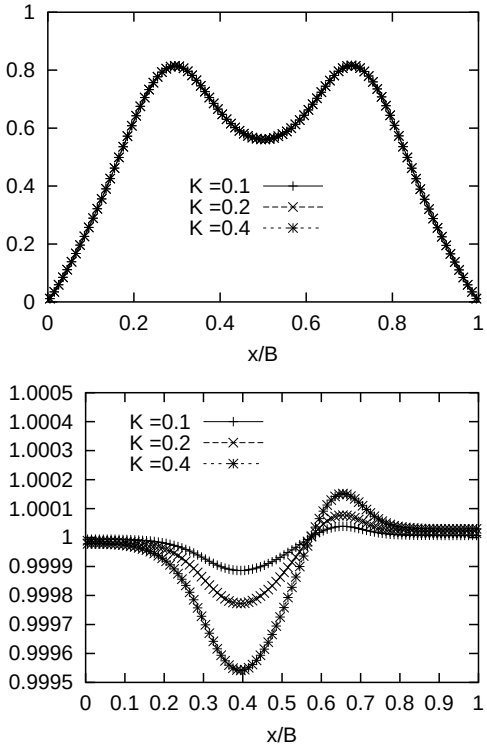

Figure 2: Time-averaged profiles of the normalized streamwise velocity v (top) and temperature T (bottom), at the plane $y/B = 1.25$. The curves depict results obtained for $K = 0.1$, 0.2 and 0.4.

Profiles of time-averaged, normalized values of the streamwise velocity and temperature are given in figure 2; profiles of the standard deviation in v and T are plotted in figure 3. The time-averaged velocity profile reflects the development of a laminar/transitional wake.

The results indicate that the mean velocity prediction is essentially independent of the coupling parameter while the uncertainty in v exhibits a significant dependence on K. This behavior is in contrast with that observed for the temperature, whose mean profile exhibits a pronounced dependence on K while the standard deviation appears to be insensitive to K. Note that the standard deviation in T follows the imposed inlet conditions, as it varies smoothly from 0 at the left boundary to 0.1 at the right wall. Meanwhile, the standard deviation in v exhibits a more complex structure, which reflects tight coupling between viscous, inertial and pressure terms.

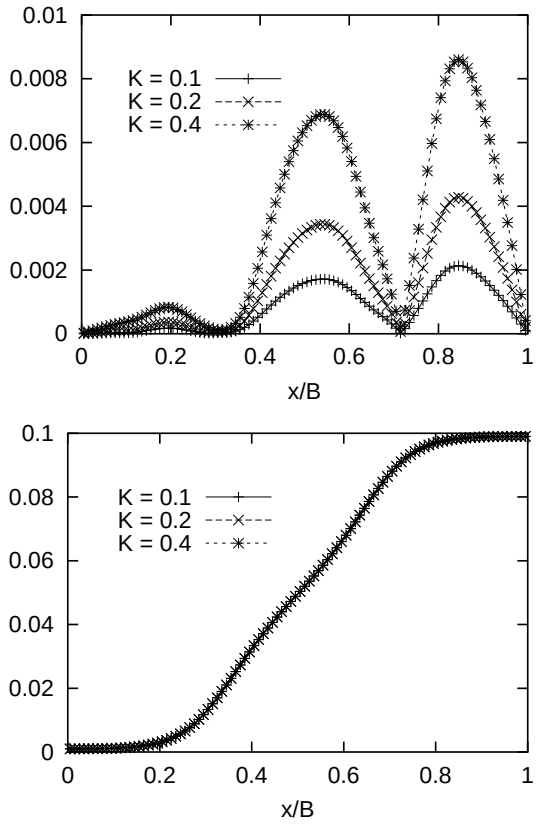

Figure 3: Time-averaged standard deviation profiles at $y/B = 1.25$ for the normalized v-velocity and (top) and temperature (bottom). The curves depict results obtained for $K = 0.1$, 0.2 and 0.4.

The complex dependence of the stochastic solution on K, as well as the appearance of node points in the standard deviation profile of v, provide an interesting example regarding possible applications of the uncertainty quantification scheme. For instance, one observes that the standard deviation in v is vanishingly small at cross-stream locations $x/B \sim 0.3$ and $x/B \sim 0.7$, where the mean signal approaches its peak value (compare figures 2 and 3). The ratio of the standard deviation to the mean value is clearly minimized at the corresponding locations. Thus, these locations constitute ideal sites for probing the streamwise velocity, in a fashion that minimizes the effect of uncertainty in the inlet temperature. This illustrates how quantitative information obtained using the uncertainty propagation scheme may be applied to system analysis and experiment design.

4 CONCLUSION

In this paper, a stochastic solver is developed which allows the propagation of uncertainty in incompressible flow simulations. The solver combines a spectral stochastic uncertainty representation scheme with a projection method for incompressible flow. Implementation of the stochastic solver is illustrated in light of transient simulations of transport and mixing in a microchannel. Attention is focused on the simplified situation where the uncertain data can be represented as a Gaussian random variable, and the resulting stochastic scheme is applied to analyze uncertainty in transport properties and boundary conditions. Work is currently underway to generalize the present formulation to situations involving reacting flow, random processes, and correlated random inputs.

ACKNOWLEDGMENT

Effort sponsored by the Defense Advanced Research Projects Agency (DARPA) and Air Force Research Laboratory, Air Force Materiel Command, USAF, under agreement number F30602-00-2-0612. The U.S. government is authorized to reproduce and distribute reprints for Governmental purposes notwithstanding any copyright annotation thereon. Computations were performed at the National Center for Supercomputer Applications.

REFERENCES

[1] Hammersley, J.M., and Handscomb, D.C., *Monte Carlo Methods,* Methuen, London, 1964.

[2] Ross, S., *Simulation,* Academic Press, 1997.

[3] Ghanem, R.G., and Spanos, P.D., *Stochastic Finite Elements: A Spectral Approach,* Springer Verlag, 1991.

[4] S., Wiener, *Amer. J. Math.*, 60:897–936 (1938).

[5] Cameron, R.H., and Martin, W.T., *Ann. Math.*, 48:385–392 (1947).

[6] Le Maître, O.P, Knio, O.M., Najm, H.N., and Ghanem, R.G., "A stochastic projection method for fluid flow. I. Basic Formulation," submitted to *J. Comput. Phys.* (2000).

[7] Chorin, A.J., *J. Comput. Phys.*, 2:12–26 (1967).

[8] Najm, H.N., Wyckoff, P.S., and Knio, O.M., *J. Comput. Phys.*, 143(2):381–402 (1998).

[9] Knio, O.M., Najm, H.N., and Wyckoff, P.S., *J. Comput. Phys.*, 154:428–467 (1999).

[10] Kim, J., and Moin, P., *J. Comput. Phys.*, 59:308–323 (1985).